LOS ALAMOS SCIENTIFIC LABORATORY
of the
University of California
LOS ALAMOS • NEW MEXICO

Internal Blast Loading of Scale-Model Explosive-Processing Bays

UNITED STATES
ATOMIC ENERGY COMMISSION
CONTRACT W-7405-ENG. 36

This report expresses the opinions of the author or authors and does not necessarily reflect the opinions or views of the Los Alamos Scientific Laboratory.

Printed in the United States of America. Available from
Clearinghouse for Federal Scientific and Technical Information
National Bureau of Standards, U. S. Department of Commerce
Springfield, Virginia 22151
Price: Printed Copy $3.00; Microfiche $0.65

Written: March 26, 1969
Distributed: July 7, 1969

LA-4145
UC-38, ENGINEERING
AND EQUIPMENT
TID-4500

LOS ALAMOS SCIENTIFIC LABORATORY
of the
University of California
LOS ALAMOS • NEW MEXICO

Internal Blast Loading of Scale-Model Explosive-Processing Bays

by

C. A. Anderson

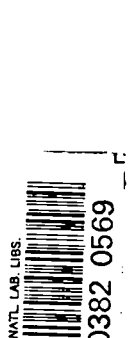

TABLE OF CONTENTS

INTERNAL BLAST LOADING OF SCALE-MODEL EXPLOSIVE-PROCESSING BAYS

by

C. A. Anderson

ABSTRACT

A Los Alamos Scientific Laboratory study of the protective capability of high-explosive-processing buildings subjected to internal blast loading is summarized. One-eighth-scale reinforced concrete models of the facility were tested against blast from a wide range of scaled explosive-charge weights. Shock overpressures, strains, and deflections were measured at critical points of the models.

The structural response of the models is compared with calculated dynamic response based on elastic and plastic material behavior, and spallation and excessive deflection of the models are compared with conventional explosive-effects data. From the test results, guide lines are established for the protection of personnel in typical Los Alamos explosive-processing buildings.

I. INTRODUCTION

In handling hazardous materials such as high explosives, great effort is expended in preventing accidents such as accidental detonations. Nevertheless, accidents can be expected to occur, however small the probability, and it is necessary to minimize their effects on personnel. Fabrication of high explosive (HE) systems involves a number of mechanical operations such as pressing, drilling, and cutting, in each of which accidental detonation can occur. In fact, a fatal accident at the Los Alamos Scientific Laboratory (LASL) involving drilling of HE prompted the study reported here.

To protect personnel from the effects of an accidental explosive detonation, it is standard practice to separate them from the potential explosion by a protective barrier, usually a reinforced concrete wall panel. If the barrier is not breached or spalled and the air shock from the explosion is channeled away from personnel, sufficient protection is ensured. Design of a protective barrier is thus well defined: it should not be breached by an explosion, should not spall, and should channel the shock wave away from personnel.

Reinforced concrete panels offer excellent protection against blast because they combine reasonable strength, ductility, mass, and economy. The ductility of correctly designed panels allows them to deflect greatly without breaking or breaching by absorbing energy through plastic flow in the reinforcing rod even though the loads greatly exceed the ultimate static carrying capacity of the panel. The use of this property of flow at constant stress without change of geometry has been incorporated in certain structural calculations for protective barriers at LASL

The difficulty in calculating an interior wall panel's response to blast loading lies in obtaining an adequate description of the pressure loading on the panel rather than in the resulting structural analysis. The pressure loading on a panel from internal blast varies with the distance of the panel from the explosion, the angle of blast incidence on the panel, and blast reflection at the panel. Additional complications are caused by shock-wave

reflections from adjacent panels as well as reflections from corners. Therefore, we turned to a model study to evaluate the protective capability of a typical LASL explosive-processing building subjected to internal blast loading.

Conclusions and recommendations obtained from the scale-model tests are given in Section II, as are guide lines for protection of personnel in a typical explosive-processing building. Hazard limits for areas adjacent to the building are also discussed.

A typical processing building is described in Section III. Sections III through VI describe the fabrication, instrumentation, testing, and test results of the two structural models used in this study. Section VII gives the measurements of pressure and impulse imparted to the models by the internal blast and the measurement of external shock-wave effects produced by the venting of the explosion through a blowout panel.

Appendix A gives the scaling laws for a shocked fluid and for the dynamic response of elastic-plastic structures. In the absence of heat conduction and rate effects, scaling of the interaction of an explosively shocked fluid and a structure can be accomplished purely geometrically; i.e., the dimensions of the explosive loading source are reduced as the geometric model-scaling factor.

Structural calculations for protective barriers at LASL are reviewed in Appendix B, and a numerical example is also given.

We emphasize that the scale-model testing treats only the problems of personnel protection and structural damage occurring in HE operating or processing buildings from the accidental detonation of modest amounts of HE within the structure. Several investigations have been made of structural response to external blast loading produced, for example, by a nuclear explosion.[1,2] Other studies, often using models, have been devoted to sympathetic detonation involving "simultaneous" initiation of explosives separated by interior dividing walls.[3] The results of this study do not apply to either of these problems.

II. CONCLUSIONS AND RECOMMENDATIONS

From the scale-model testing described in this report we have arrived at the following conclusions and recommendations about the protective capability of typical LASL explosive-processing buildings.

A. Protection Afforded by a Typical Structure

1. Breaching Detonation of more than 400 lb of plastic bonded explosive (PBX 9404) would be required to breach (completely break up) a typical LASL explosive-processing bay. The scale-model blast from a 370-lb-equivalent weight of PBX 9404, although inflicting extensive damage to the model, was contained by its processing bay.

2. Spallation Some investigations[4] indicate that spallation of reinforced concrete can be avoided if the explosive is kept a scaled distance, $R/W^{\frac{1}{3}}$, of at least 1.5 from the concrete. (R is the distance from the concrete in feet, and W is the explosive weight in pounds.) From our scale-model tests, it appears that this requirement has a considerable safety factor, and that a smaller scaled distance could be used. We observed spalling in our scale-model tests (W and R are actual, not scale-model figures) as follows:

Test	W	R	$R/W^{\frac{1}{3}}$	Spallation
47	125	2	0.40	Yes
48	100	3	0.65	No
57	200	5	0.83	No
58	370	5	0.70	Yes

Spallation is to be avoided for the safety of personnel in corridors.

3. Overpressures The shock overpressure in the processing bay adjacent to that in which the detonation occurred indicated that if a mechanical operation is considered hazardous enough to be done remotely, personnel should not be allowed in the adjacent bay. The overpressures behind the remote control barrier of the model were considerably less than those in the adjacent corridors. For charge weights of less than 25 lb of PBX 9404, all corridor pressures are less than 5 psi.

4. The Effect of Blast Doors Blast doors can effectively seal off the personnel corridors, and probably should be used for processing of charges exceeding 25 lb of PBX 9404.

5. The Effect of a Blowout Panel A blowout panel did not seem to affect the model structural response, although corridor and adjacent bay pressures were considerably less without it. This was confirmed by the impulse measurements which

showed that the impulse applied to the structure was substantially the same with or without a blow-out panel.

B. Structural Response

The entire model structure behaved elastically up to the equivalent of 50 lb of PBX 9404 with no permanent deformation of the wall and roof panels. Maximum elastic panel deflections of 3/16 in. (1-1/2 in. in the full-scale building) occurring 1 to 2 msec after detonation were measured in the model. Except for one instance of spallation the thick, heavily reinforced walls of the model behaved elastically even at the 125-lb-equivalent charge level, with some minor cracking occurring at the 200-lb-equivalent charge level. The model roof panel, being thinner than the supporting side walls, was much more deformed and behaved as expected, with clear evidence of purely elastic, elastic-plastic, and fully plastic regions of behavior. Finally, it appeared from analysis of the test records that the impulse delivered to the reinforced concrete wall and roof panels of a structure is the primary cause of deflection and that the exact shape of the pressure-time loading function is unimportant.

C. Personnel Effects

Various figures are given for the adverse effects of shock overpressures on personnel. From a Lovelace Clinic report[5] it is apparent that severe internal injuries from a conventional explosive charge require a uniform overpressure of hundreds of pounds per square inch (a man is reported to have survived an estimated 500-psi pressure from a World War II bomb burst) provided that the duration is short--of the order of tens of milliseconds. No pressures measured in the model corridors even approached this range. The part of the human anatomy most sensitive to overpressure is the eardrum, for which 2 to 40 psi cause rupture. A value of 5 psi appears reasonable, and was used for the recommendation concerning blast doors.

A human dummy, placed in an extension of the model personnel corridor, was unaffected by the 25-lb-equivalent charges but was upset by 50-lb-equivalent and greater charges. The dummy always fell in the direction of shock propagation although no translational velocity was observed. From high-speed films, it appeared that the dummy did not respond to the impulse of the initial shock but, rather, to the dynamic pressure of the longer duration, forward-moving wind accompanying the shock.

D. Significance of Calculations

Structural response calculations based on the simplified elastic, perfectly-plastic model described in Appendix B appear to agree well with the structural response of the scale-model roof panel, provided that the pressure-loading function or impulse acting on the panel is known. For calculational purposes estimates of this pressure-loading function were obtained by using reflected impulse values for the distance from the nearest point on the panel to the center of the explosive[6] and assuming that the impulse acted simultaneously and uniformly over the panel. For large deflections of the model structure, in addition to bending, it appeared that membrane effects should be accounted for in the response of the theoretical elastic, perfectly-plastic model; significant curvature in the model roof panel indicated the presence of membrane forces.

E. Reflected Impulse and External Overpressures

1. Reflected Impulse In assessing the effects of blast on structures, one must distinguish between peak pressure and positive impulse in free undisturbed air ("side-on" pressure and impulse) and the peak pressure and positive impulse applied to an infinitely rigid wall at normal incidence ("face-on"). For internal blast loading, the normally reflected (face-on) pressure and impulse are the important parameters. Measurements of the reflected impulse applied to the walls of the model were in fair agreement with published reflected-impulse data.[6] Although reflected peak pressures varied considerably over the internal surface of the model, the reflected-impulse values were distributed fairly uniformly. The influence of the location of the explosive within the model on the resulting overpressure and impulse distribution was also characterized by considerable variations in peak reflected pressures and a fairly uniform impulse distribution.

2. External Overpressures As expected, shock overpressures measured outside the model

in front of the blowout panel depended strongly on the distance from the explosive charge, with a smaller pressure variation with angle at a fixed radius. For the equivalent of 25 lb of PBX 9404, an equivalent of 50 ft from the charge will ensure that the peak overpressures are less than 5 psi (side-on). The 100-lb-equivalent charge of PBX 9404 produced pressures of over 5 psi at 100 ft, the greatest equivalent distance at which external pressure measurements were taken. We consider 5 psi without shrapnel the peak overpressure safe for personnel.

F. Comparisons with Conventional Explosive-Effects Data

Reflected impulses from normal incidence of blast waves generated by PBX 9404 were 30% greater than the corresponding impulses from TNT, and the reflected peak overpressures were 10 to 20% greater. As mentioned, the reflected impulse values agreed fairly well with published values. External peak shock overpressures measured near the blowout panel were about twice those given by the Explosion Effects Data Sheets[7] for TNT. This we attribute to the use of a higher energy explosive and to the fact that the air blast was directional in nature. We also found that internal shock overpressures in corridors and entryways could be estimated from the Explosion Effects Data Sheets by using the distance of shock travel together with the explosive weight even though the blast is no longer spherically divergent. These data afford a crude practical rule for estimating shock overpressures in personnel areas of other types of processing buildings.

III. THE STRUCTURAL MODELS

After considering the scaling laws developed in Appendix A, we decided to construct one-eighth-scale structural models of part of a typical LASL explosive-processing building and to subject them to internal blast loading from scaled explosive charges. The tests would determine the structural resistance of the processing building to internal blast loading and its ability to channel the explosion shock waves away from personnel.

A typical explosive-processing building consists of 25 bays in which mechanical operations on explosives are performed. The bays are arranged in pairs, with a single end bay, and with a common wall separating adjoining pay pairs. The floor plan of a typical bay pair is shown in Fig. 1. The supporting walls of the bays are 12-ft-high, 2-ft-thick, heavily reinforced concrete with 3 to 4 vol % of reinforcement. The bay is covered by a 15-in.-thick reinforced concrete roof panel (~3 vol % reinforcement) with substantial support at three edges. The wall and ceiling corners are haunched to provide there an approximately built-in support. The concrete floor of each bay "floats" on an earth fill. As shown in Fig. 1, the back of the bay pair is covered by a light frangible blowout panel to vent the blast from an accidental detonation and provide protection from weather during ordinary operation. The panels are two 1/16-in.-thick aluminum sheets with their 3-in. separation filled with insulation. Since most operations on explosives are remotely controlled, a "remote control" protective barrier for the operator is provided as shown in Fig. 1. During a mechanical operation on an explosive, personnel are restricted to areas behind the remote control barrier and to the personnel corridor.

The two structural models for this study were based on the bay pair shown in Fig. 1. The testing of each model would be an overtest of the actual building since we felt that adjoining bay pairs would contribute somewhat to the strength of an actual bay pair. Each model was a one-eighth scale geometric replica of a bay pair. It was often difficult to simulate in the model the exact placement and size of the reinforcing bar in the building; in these cases the available scaled reinforcing bar was positioned in the model so that the ratio of the ultimate plastic moment of the building section to that of the corresponding section of the model was 64 as dictated by the scaling laws.*

To maintain proper scaling, the mechanical properties of the materials making up the model must be held close to their values in the actual structure. To this end much effort was expended in scaling aggregate and duplicating strength values; the strength of the 3/32-, 1/8-, and

*For example, the ultimate plastic moment of a uniform section is $\sigma_o h^2/4$, where σ_o is the tensile (and compressive) yield strength and h is the section thickness. If the model section thickness is λh, its ultimate plastic moment is $\lambda^2(\sigma_o h^2/4)$. The same holds for composite sections.

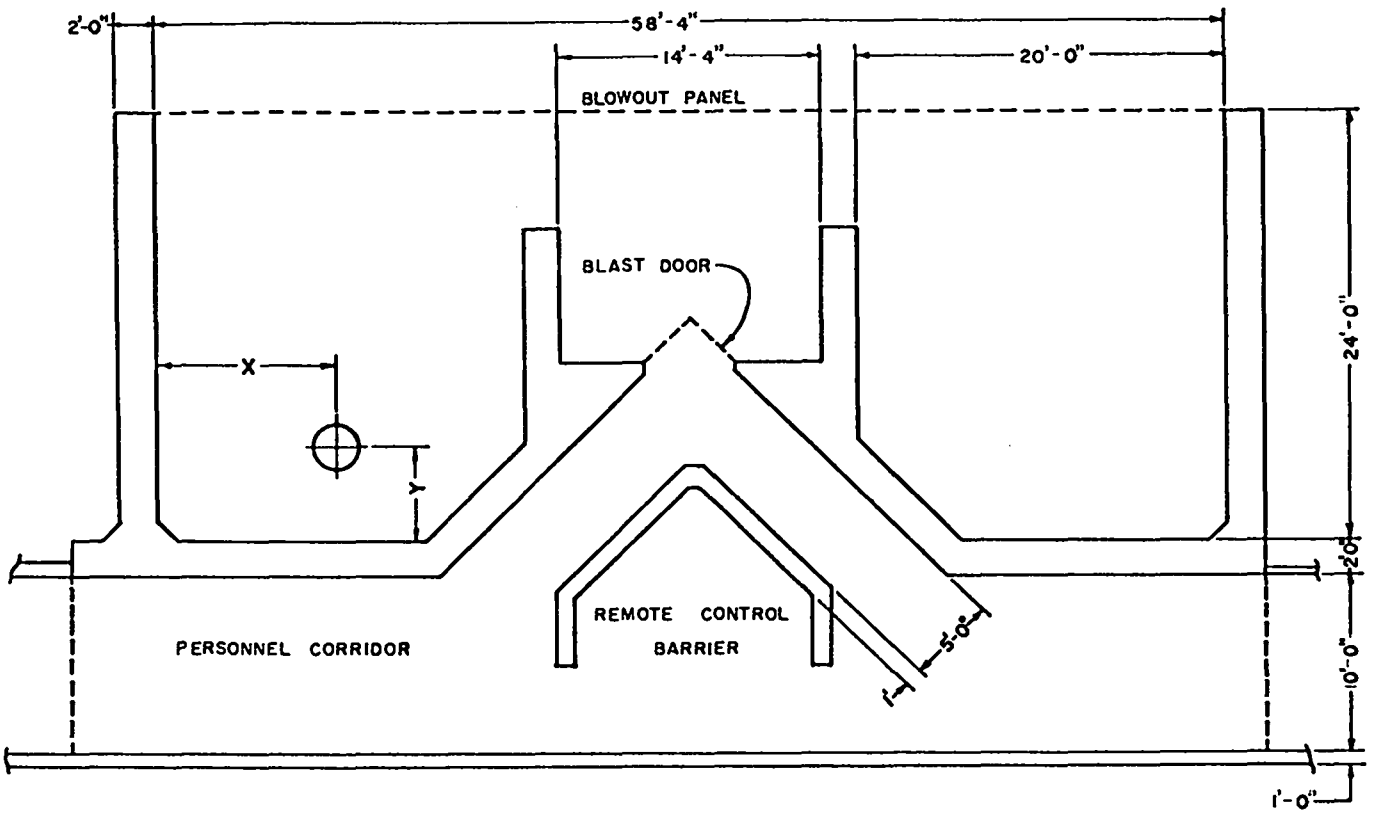

Fig. 1. Floor plan of a typical processing bay pair. X and Y coordinates are used to indicate charge location.

3/16-in. round and square wire rod simulating the reinforcing bar of the building was adjusted by annealing the wire to the desired tensile yield strength. The strengths of the concrete and reinforcing bar in the two models compared with those in the building are as follows.

Mechanical Property	Model 1 (psi)	Model 2 (psi)	Actual Building (psi)
Concrete compressive strength at 7 days, σ_o	3,800	3,800	
Concrete compressive strength at time of model tests	6,600	6,600	6,000
Tensile strength of reinforcing bar, σ_y	68,000	45,000	49,000
Ultimate strength of reinforcing bar, σ_u	80,000	72,000	75,000

The elastic properties of the materials making up the models were substantially the same as those of the actual building. Typical stress-strain curves for the reinforcing bar and concrete are shown in Fig. 2.

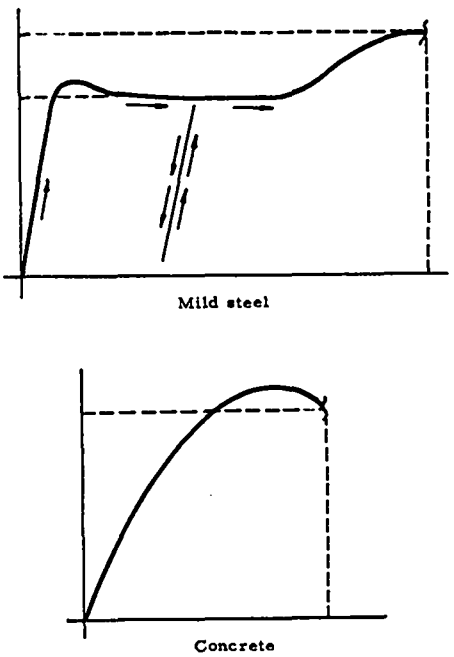

Fig. 2. Typical stress-strain curves for mild steel and concrete.

As shown above, the second structural model is a more accurate strength simulation of the actual bay pair than is the first. Also the first model had a built-in condition at its base which did not simulate a foundation-type support; the second model attempted to correct this shortcoming.

The models had simulated blowout panels consisting of three pieces of 1/32-in. aluminum sheet stock held in place by pressure-sensitive tape. The equivalent weight of the model panel exceeded the weight of the actual panel by about 50%. The amount and placement of the pressure-sensitive tape were adjusted so that the model blowout panel response to a 5-lb-equivalent charge simulated some known actual panel response.

Figures 3 through 6 show the structural models in three phases of construction. Fig. 3 shows the detailed placement of the wire reinforcing bar in the walls of the two bays and the remote control barrier, while Fig. 4 shows the intricate detail of the reinforcement at a typical corner. Figure 5 shows a partially completed model with the forms for pouring the concrete. Figure 6 shows the completed model ready for instrumentation and testing. Details of the two structural models are given in LASL drawings ENG C-26468 through ENG C-26477.

IV. MODEL INSTRUMENTATION

We wished to measure dynamic strain, incident and reflected shock overpressures, and wall- and roof-panel motion in the structural models. Strain gages were bonded to the outer reinforcing bars embedded in the wall and roof panels at 16 locations where maximum strain was anticipated. These gages were 120-Ω, Bakelite-backed gages, 0.060-in. long, suitably waterproofed for use in concrete. In the first model, the gages were mounted on both vertical and horizontal reinforcing bars of the walls, whereas on the second model they were mounted only on the vertical bars. The strain-gage locations in one of the model bays are indicated in Fig. 7.

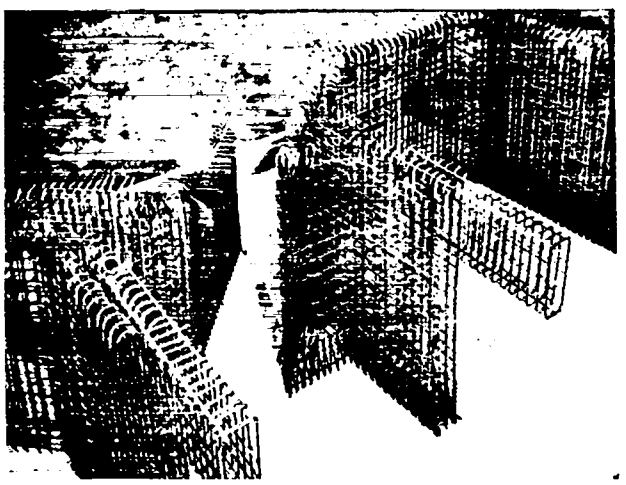

Fig. 3. Reinforcing bar assembly showing adjacent model bays and remote control barrier.

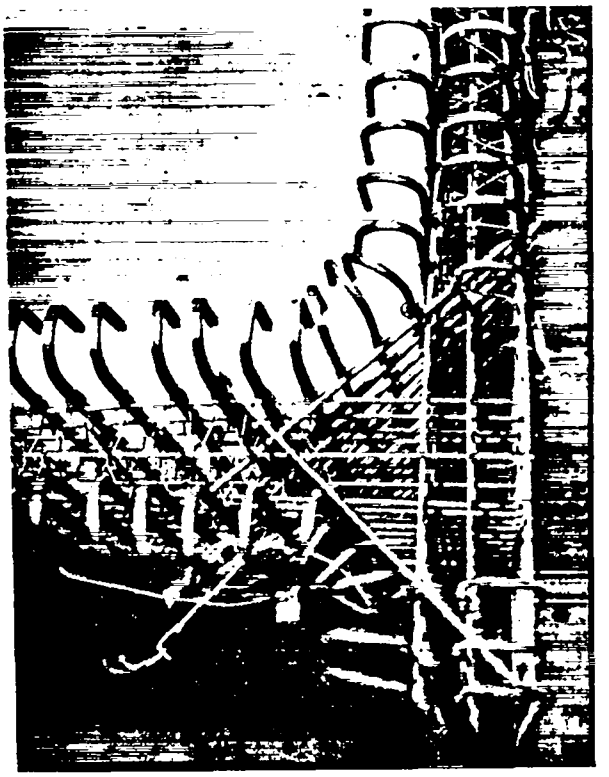

Fig. 4. Reinforcing bar detail at a typical corner.

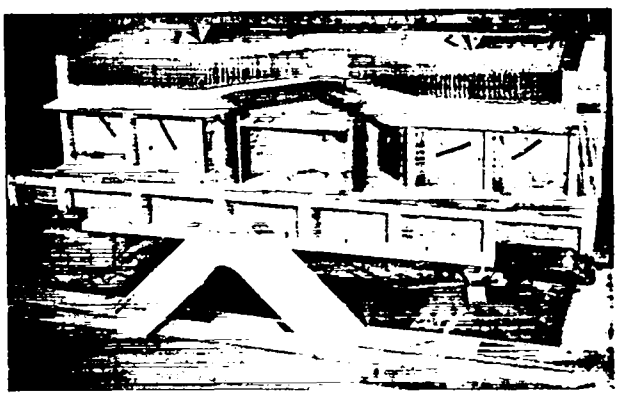

Fig. 5. Model assembly before concrete pouring.

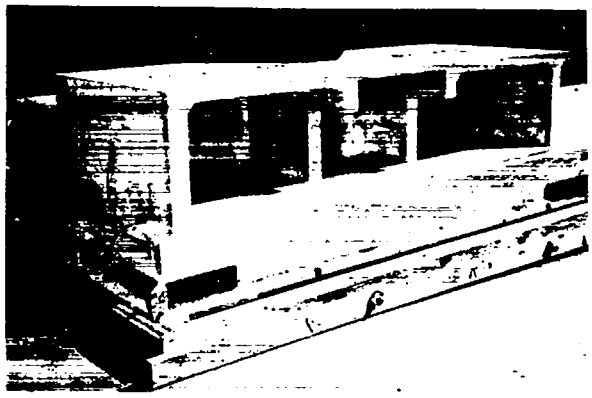

Fig. 6. Structural model ready for instrumentation and testing.

Shock overpressures throughout the structural model were measured by 14 Atlantic Research Corporation blast gages positioned as shown in Fig. 7. These gages presented a small frontal area to the incident flow and so perturbed the flow only slightly in their measurement of the incident free-field shock overpressure. The gages had a natural frequency over 100 kc with a sensitivity of approximately 500 pC/psi. Calibration of the blast gages with a step pressure change indicated linearity of response within ±5% for the range of pressures of interest. The blast gages were mounted on stands so that the gage itself was 6 in. above the floor of the model. None was placed in the bay in which the explosion took place.

Since we anticipated difficulties in measurement of wall- and roof-panel motion, we used two methods of measurement. High-speed cameras recorded the motion of pointers attached to the midpoints of the roof panel and side wall of the bay in which the explosive was detonated. The camera framing rate was approximately 6000 frames/sec. In addition, six Bently Nevada Corporation motion detectors measured the wall- and roof-panel motion in the 0- to 0.250-in. maximum deflection range. The frequency response of these detectors was somewhat limited for our applications, and some distortion of their signals was observed. Of course, permanent deformation of the structure by large-scale charges provided a measure of maximum deflection, particularly when the permanent deformation was large compared with the elastic deformation measured at low charge levels.

Reflected wall pressures and impulse were measured with quartz pressure transducers purchased from pcb Piezotronics, Inc. These transducers were mounted flush with the inside surfaces of the walls and roof of a geometric steel model of the bay in which the explosion took place (see Section VII). The transducers can measure pressures up to 5000 psi with less than 2% nonlinearity of response. The transducer sensitivity is 0.4 pC/psi, and they have an extremely high natural frequency (about 400 kc) which enables them to record accurately the severe shock signature caused by the reflection of the blast wave from the walls and roof of the model.

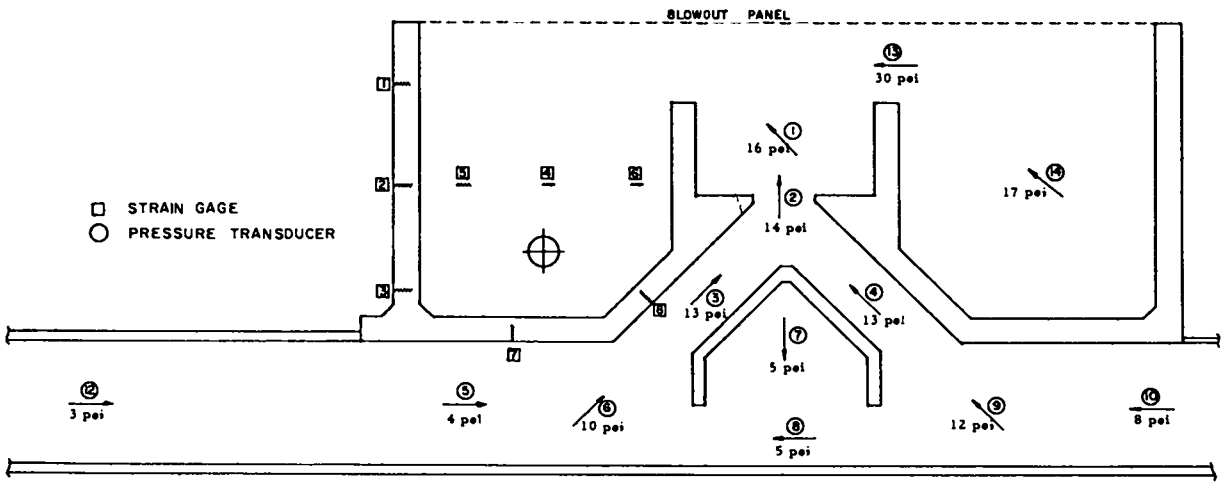

Fig. 7. Map of shock overpressures from 75-lb-equivalent charge, Test 55.

The signals from the strain gages, pressure gages, and motion detectors were recorded on a cathode-ray oscillograph, or oscilloscopes, or both after appropriate signal conditioning.

V. MODEL TESTING

The two structural models were tested at scaled explosive-charge levels of 25- to 370-lb-equivalent weights of a high explosive, PBX 9404. The weight of explosive detonated in the model ranged from 22 to 325 g, determined by reducing the full-scale charge weight by 512 (the scaling factor cubed). All charges were positioned a scaled 4 ft above the model floor, corresponding to average machining table height. Use of an SE-1 detonator ensured complete detonation of the scaled charge.

For the first structural model, hemispherical charges of PBX 9404 were employed, beginning with the 25-lb-equivalent charge. Firing of multiples of the 25-lb-equivalent charge followed until substantial damage to both bays of the model was observed. The blowout panel was used for all of the explosive tests on the first structural model. No tests of the first structural model employed blast doors. The amount and horizontal location of each explosive charge relative to the actual structure is indicated in Table I.

TABLE I

Tests of First Structural Model

Test	Full-Scale Charge (lb)	Scaled Charge (g)	Charge Placement Coordinates (ft) (See Fig. 1) Bay	X	Y
45	25	22	B	10	12
46	50	44	B	10	12
47	125	110	A	2	12
48	100	88	B	10	3
49	125	110	B	10	3

The test program for the second structural model is given in Table II. Here cylindrical charges of PBX 9404 were used. The detonation of the two large charge equivalents, Tests 57 and 58, ensured that the structure was driven well into the plastic range of behavior. In Test 51, we examined the structural response of the model to a 25-lb-equivalent charge without the blowout panel. All other tests employed the blowout panel. In Test 52, blast doors were placed over the entryway to the corridor (see Fig. 1).

TABLE II

Tests of Second Structural Model

Test	Full-Scale Charge (lb)	Scaled Charge (g)	Charge Placement Coordinates (ft) (See Fig. 1) Bay	X	Y
50	25	22	A	10	12
51	25	22	A	10	12
52	25	22	A	10	12
53	25	22	B	10	12
54	50	44	A	10	12
55	75	66	B	10	12
56	125	110	B	10	5
57	200	176	A	10	5
58	370	325	B	10	5

To obtain more extensive shock overpressure measurements in the personnel corridor of the model, we extended the corridor by adding a 15-in.-square, 7-ft-long duct at each end. The ducts did not simulate structural response; they were only to channel the shock wave from the explosion a greater distance within the confines of the duct. One of the ducts was fitted with a transparent panel to permit a high-speed camera to record the movement of small vertical threads spaced at 2-in. intervals along the duct.

The camera simultaneously recorded the response of a one-eighth-scale human model to the incident shock wave and following air flow. The properties of the rigid-body dummy placed in the add-on corridor are as follows:

Weight	~0.4 lb
Projected frontal area	13 in.^{2}
Center of pressure of projected area	4.5 in. from the base
Radius of gyration about the base	5.0 in.

Figure 8 shows the second structural model with the add-on ducts in place and with a blast shield, shown on the left, which was used to keep the detonation products out of camera view. Some of the instrumentation discussed in Section IV can also be seen.

Testing of both structural models was performed outdoors. The first model was tested during March 1963; the second, during October 1968.

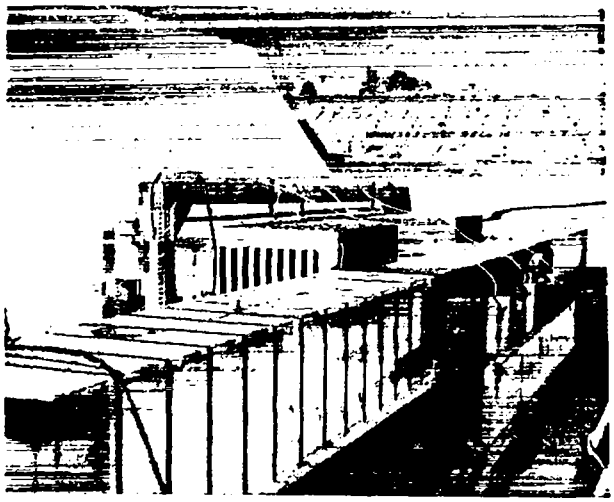

Fig. 8. Instrumentation setup before a scale-model test showing the blast shield and add-on corridors.

The air temperature during testing of the second model varied from 54 to 80°F; the atmospheric pressure was 11.1 psi.

VI. MODEL TEST RESULTS

A. Tests 45 and 50 through 53 (25-lb HE equivalent)

Since the entire model structure behaved elastically and returned to its initial configuration after blasting of the 25-lb-equivalent charges, repeated tests were conducted at this level to check instrumentation and verify certain hypotheses about structural response. Maximum strains in the reinforcing bar of the model wall and roof panels are summarized in Table III.

TABLE III

Maximum Strains (μ in./in.) from 25-lb Equivalent Charge at Positions Indicated in Fig. 7

Test	Average of Positions 1 - 3	Position 4	Position 7	Position 8
45	560	1610	300	200
50	330	1320	280	470
51	250	1370	260	190
52	320	1440	300	380
53	450	1340	410	370

Since the roof-panel strains recorded in Table III (position 4) are approximately the same, we conclude that at the 25-lb-equivalent charge weight the presence or absence of the blowout panel, or blast doors, or both has little effect on the structural response. The motion transducers indicated an average maximum displacement of 1/8 in. at the center of the roof panel.

B. Tests 46 and 54 (50-lb HE equivalent)

No structural damage was observed on Tests 46 and 54; the structure behaved elastically and returned to its original configuration. A maximum roof-panel deflection of approximately 3/16 in. was recorded on Test 54, and the maximum strain recorded in the reinforcing bar at the center of the roof panel slightly exceeded the yield-point strain.

C. Test 55 (75-lb HE equivalent)

The 75-lb-equivalent charge was the lowest charge weight at which permanent deformation of the model was observed; the roof panel of the bay being tested showed evidence of the formation of plastic hinges with a 1/8-in. permanent deflection of its central yield line. The thicker walls of the model showed purely elastic behavior, although there was some cracking at the support.

D. Test 48 (100-lb HE equivalent)

Severe cracking at the edge of the roof panel as well as the formation of plastic yield lines occured as shown in Fig. 9. The permanent deflection was 5/32 in. at the center of the roof panel. No spallation was observed, and the walls of the model behaved elastically.

E. Test 47 (125-lb HE equivalent)

Figure 10 illustrates the damage to the model caused by a 125-lb-equivalent charge placed a scaled 2 ft away from a side wall panel of the actual building. The only damage to the side wall

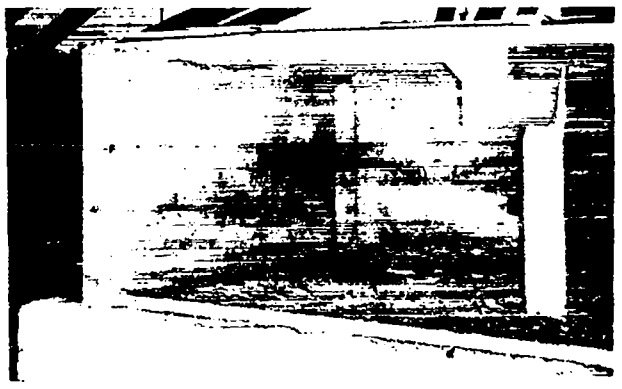

Fig. 9. Damage to the first structural model, Test 48.

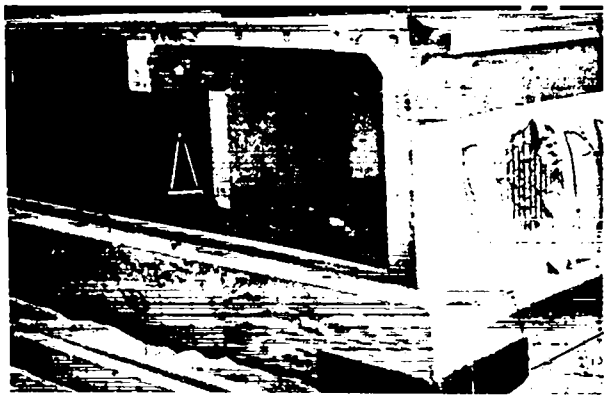

Fig. 10. Spalling of the first structural model, Test 47.

was spallation, whereas the roof panel cracked at the spalled wall-roof interface, probably because of large transverse shear stresses.

F. Test 49 (125-lb HE equivalent)

Test 49 with a 125-lb-equivalent charge was conducted in the same bay as Test 48, and accentuated the effects of Test 48. Appreciable transverse shear effects are seen in Fig. 11 as is the absence of wall failure. No spallation was observed although the charge was detonated only a scaled 3 ft from the actual corridor wall. We feel that the shear effects observed in the first structural model would not have occurred if the yield strength of the reinforcing bar had been lowered to the value achieved in the second model.

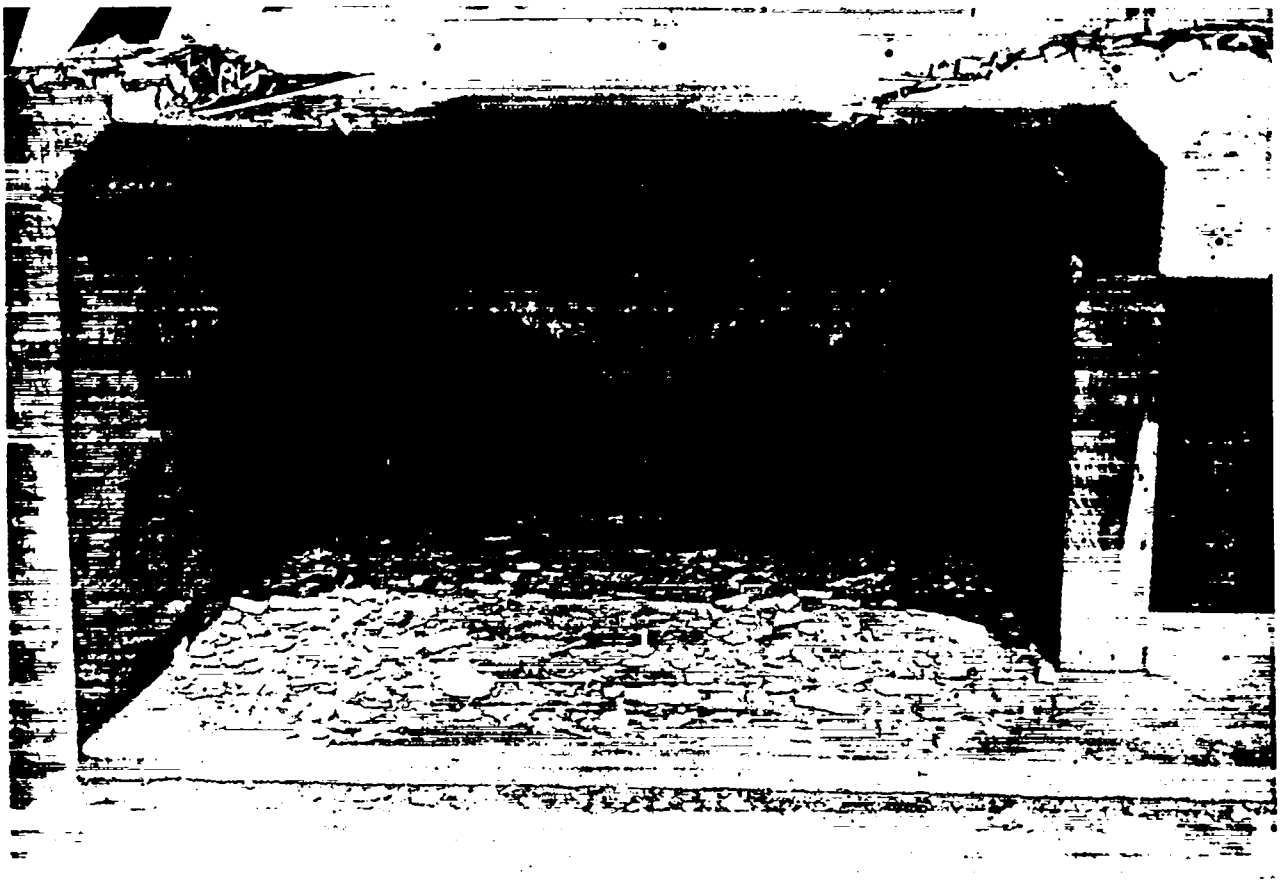

Fig. 11. Damage to the first structural model, Test 49.

G. Test 56 (125-lb HE equivalent)

Yield hinges and a yield-line pattern on the roof panel were clearly visible after this test. The permanent deflection of the roof panel was 3/8 in. (1/4 in. relative to the undeformed bay because Test 55 had already produced 1/8 in. permanent deformation of the roof panel). No permanent deformation of the side and corridor walls was observed, although large cracks appeared at the foundation of the model as shown in Fig. 12.

H. Test 57 (200-lb HE equivalent)

A definite yield-line pattern was observed on the roof panel, with a permanent deflection of 7/16 in. This pattern, shown in Fig. 13, agrees with that predicted by rigid-plastic theory (see Appendix B). Small cracks on the side wall indicated the beginning of a yield-line pattern there

Fig. 12. Cracking at the foundation of the second structural model, Test 56.

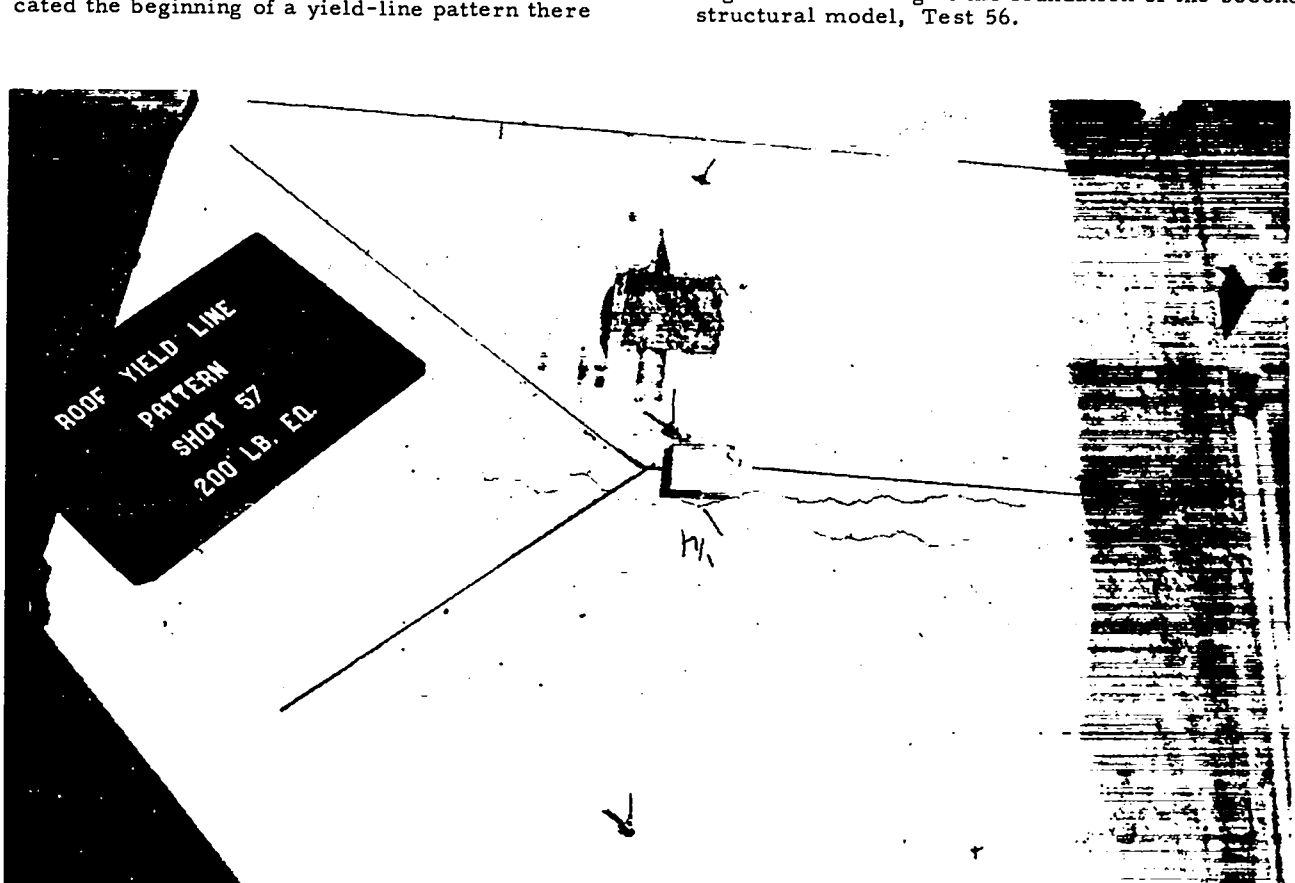

Fig. 13. Yield-line pattern initiated in the roof panel of the second structural model, Test 57.

too. This test damaged the floor considerably, and the outside wall as a whole rotated due to loss of integrity of the simulated foundation (Fig. 14). No spallation was observed in this test. The add-on corridors (which were not a structural simulation) and the blast shield were collapsed by the shock overpressures.

I. Test 58 (370-lb HE equivalent)

Test 58 with a 370-lb-equivalent charge drove the structure well into the plastic range of behavior, with excessive cracking and spalling of both the wall and roof panels of the bay. Figure 15 shows the interior of the bay and cracks which formed in the ceiling and the damage to the floor of the model. The yield-line pattern initiated by Test 56 was carried much further by this test; however,

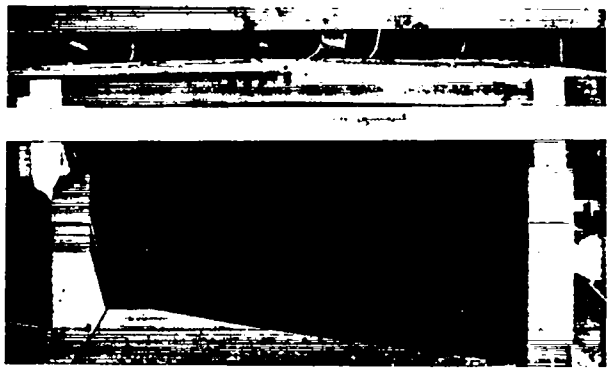

Fig. 14. Further evidence of the yield-line pattern after Test 57.

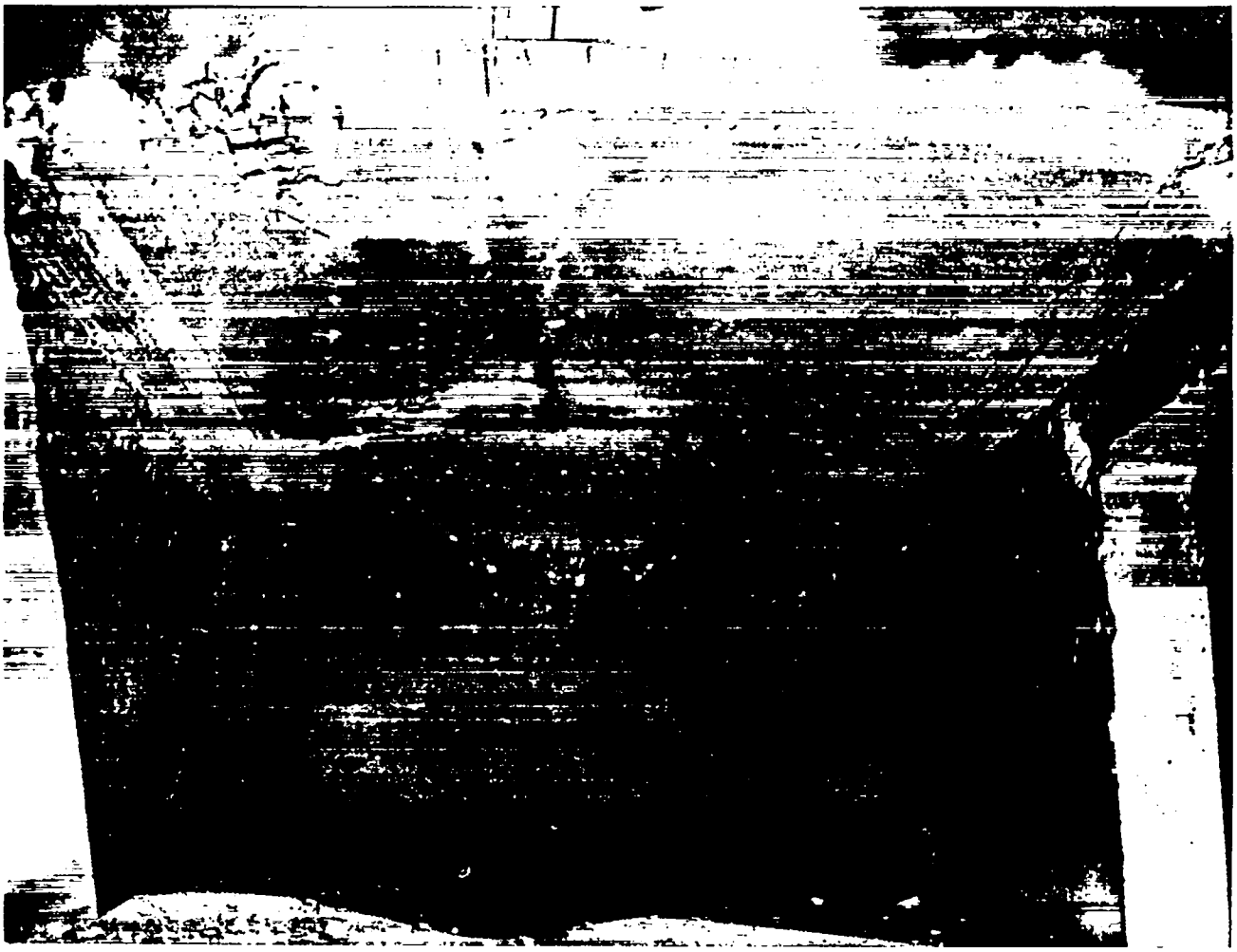

Fig. 15. Interior view of model damage caused by Test 58 showing extensive cracking of the model and roof panel curvature.

the curvature of the roof panel indicated in Fig. 15 suggests that large membrane stresses are beginning to act and that geometry changes are no longer insignificant. The permanent deflection of the model roof panel was 1-1/4 in. Figure 16 illustrates the crack pattern and spallation of the roof panel, and Fig. 17 shows the corridor wall spall. The high-speed camera records indicated spall velocities of about 100 ft/sec. Figure 18 shows the model after the completion of the test series; we emphasize that in spite of the severity of the 370-lb-equivalent test the model structure was not breached.

J. Summary of Test Results

Figures 19 through 21 summarize the structural data obtained from testing both models, with the quantities of interest plotted against equivalent weights of PBX 9404 detonated in the actual structure. We mention again that according to the scaling laws the strains, being dimensionless, are the same in the model and actual structure, and the deflections of the actual structure are eight times the values measured in the model.

The experimental values of maximum roof-panel displacement plotted in Fig. 19 are averages obtained with the 25- and 50-lb-equivalent charges. For larger equivalent charges, the deflection is the sum of the observed permanent deflection and an elastic deflection of 3/16 in. Figure 19 also shows the calculated maximum panel displacement based on the elastic, perfectly plastic model discussed in Appendix B. The measured displacements agree well with calculation. The material behavior regions of the roof-panel response are

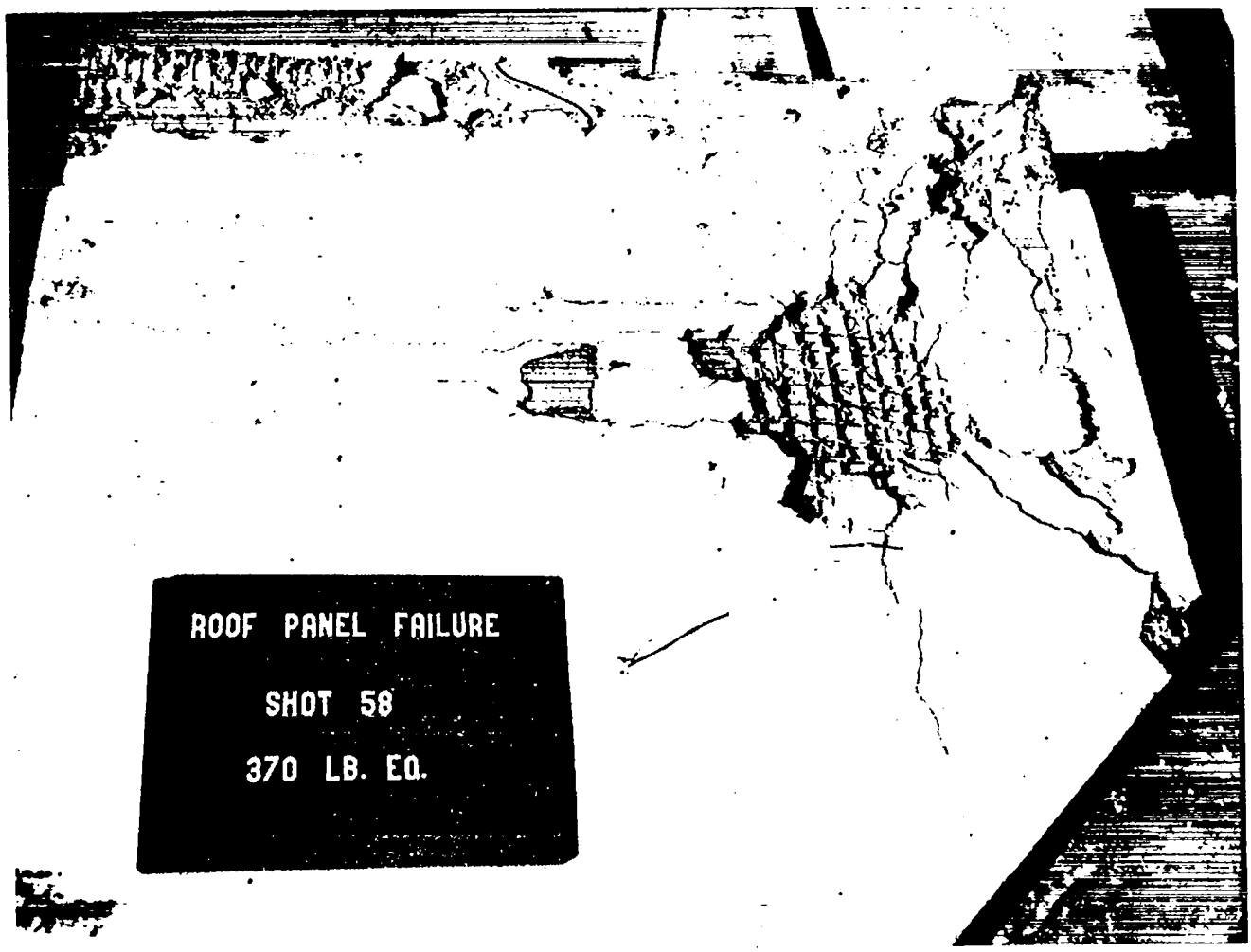

Fig. 16. Roof panel spall, Test 58.

Fig. 17. Corridor wall spall, Test 58.

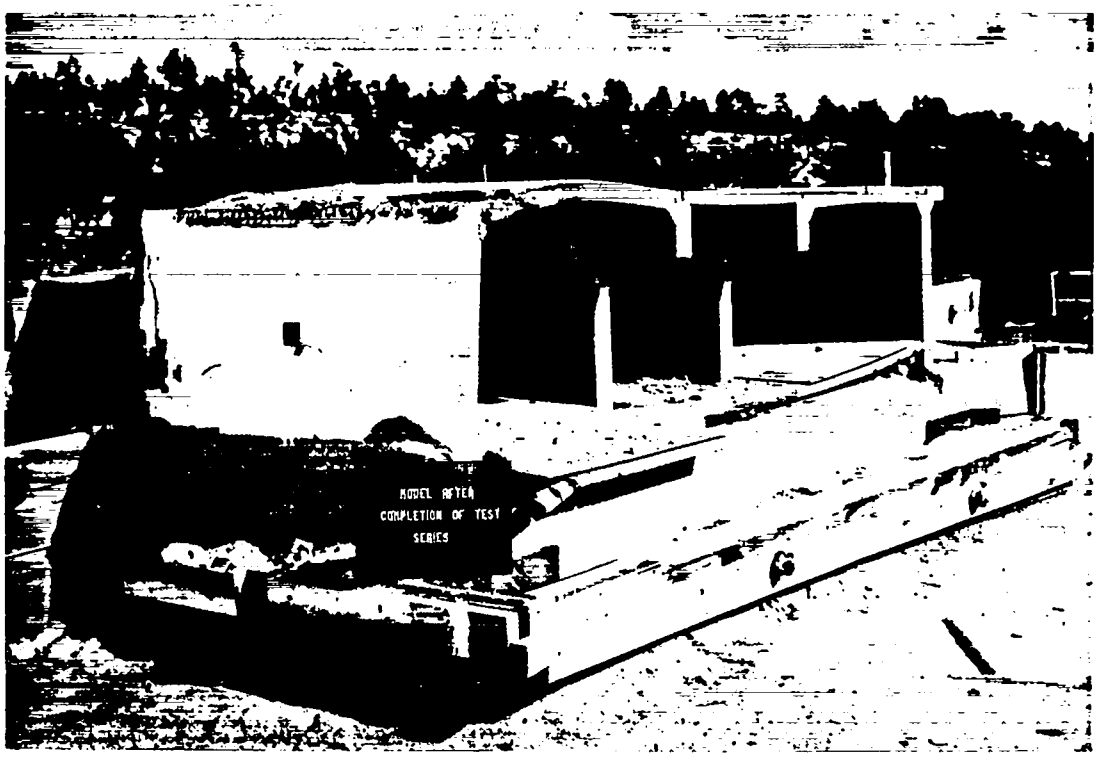

Fig. 18. Second structural model after completion of the test series.

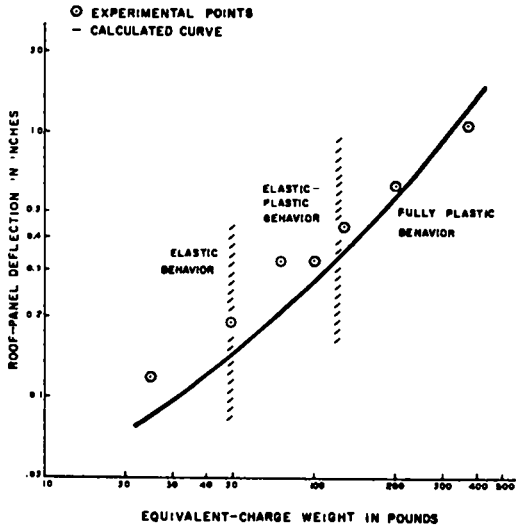

Fig. 19. Maximum deflection of the model roof panel as a function of equivalent-charge weight of PBX 9404.

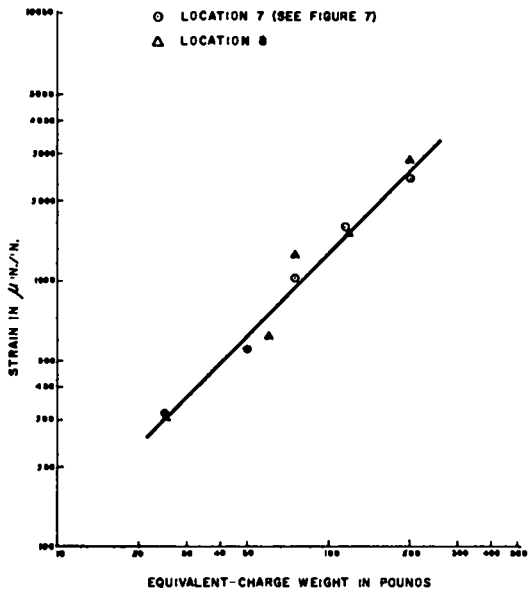

Fig. 20. Maximum corridor wall strain versus equivalent-charge weight of PBX 9404.

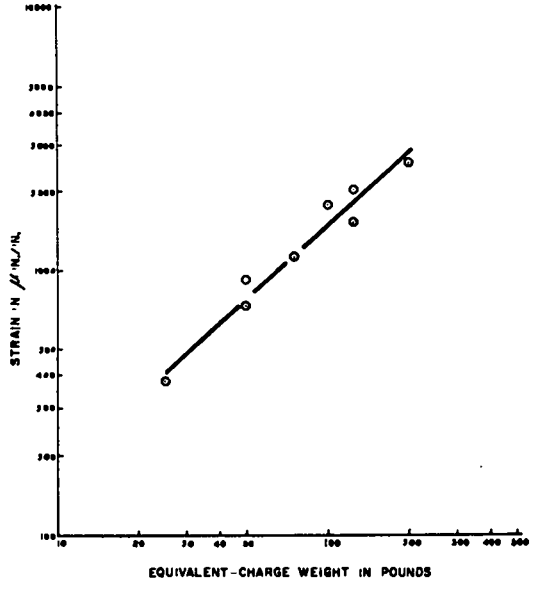

Fig. 21. Average side wall strain versus equivalent-charge weight of PBX 9404.

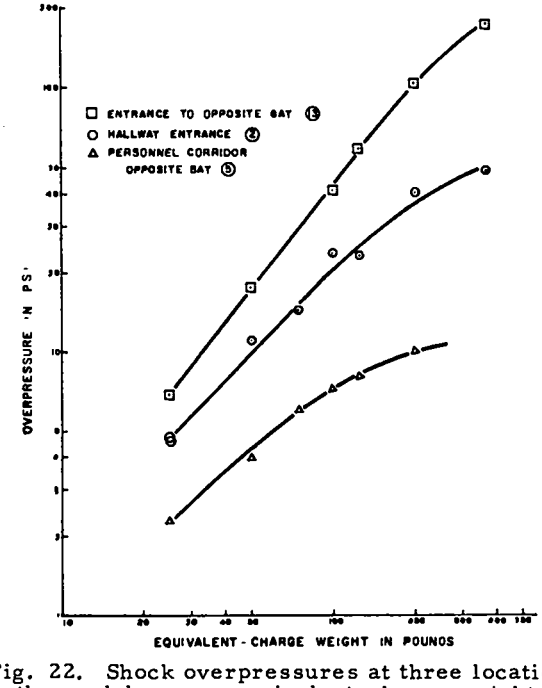

Fig. 22. Shock overpressures at three locations in the model versus equivalent-charge weight of PBX 9404. The numbers in circles are pressure transducer locations from Fig. 7.

also indicated: with up to 50-lb-equivalent charges, the structure behaved elastically with a maximum roof-panel deflection of 3/16 in.; from 50 to 125 lb, the plastic (or permanent) deflection was less than twice the maximum elastic deflection (3/16 in.); and with greater than 125-lb-equivalent charges the permanent deflection exceeded twice this elastic deflection.

Figures 7 and 22 summarize the free-field shock overpressures measured within the model in Tests 45 through 58. Figure 7 is an overpressure map at the 75-lb-equivalent charge weight (recall that shock overpressures are the same in model and prototype). In Fig. 22 the overpressures measured at three locations in the model are plotted as a function of equivalent-charge weight. Shock velocities computed from differences in shock arrival times agreed well with those computed by use of the Rankine-Hugoniot relations and the measured shock overpressures.

Figure 23 shows typical overpressure, deflection, and strain oscillograph records made in Test 51. The deflection and strain oscillograph traces are from the gages located at the center of the roof panel, and the overpressure measurement was taken at Station 1 (Fig. 7). From the half-period of the deflection oscillograph record, we conclude that the fundamental resonant frequency of the roof panel was approximately 170 cps.

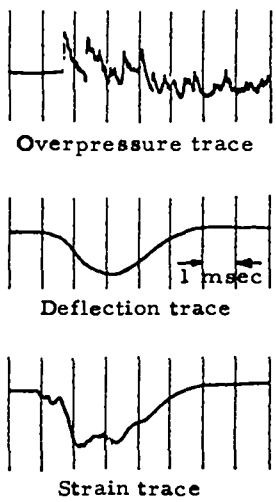

Fig. 23. Typical overpressure, deflection, and strain oscillograph records from Test 51.

The human model was unaffected by the corridor overpressure generated by the 25-lb-equivalent charge, but was upset by the 50-lb and greater charges (always falling in the direction of propagation of the shock) although no translational velocity of the model was observed. From an examination of the high-speed films it appeared that the model did not respond to the impulse of the initial shock but rather to the dynamic pressure associated with the longer duration, forward-moving "wind" or possibly to the ground shock generated by the explosion. For example, the wind (particle) velocity for the incident 8-psi overpressure air shock measured in the corridor during Test 57 was approximately 500 ft/sec, and the associated dynamic pressure ($1/2\ \rho V^2$, where ρ is the density of air and V is the particle velocity) was 1 psi. The high-speed movies focused on the particle motion indicators in the add-on corridor indicated a positive wind phase duration of approximately 13 msec at this overpressure value.

Finally, we were able to determine from films (144 frames/sec) of the blowout panel response approximate initial velocities of the blowout panel at some smaller equivalent-charge weights. For the 25- and 75-lb-equivalent charges, the initial velocities were 300 and 500 ft/sec, respectively; for a 5-lb-equivalent charge, we observed an initial velocity of approximately 80 ft/sec.

VII. IMPULSE AND EXTERNAL PRESSURE MEASUREMENTS

Reflected wall pressure and positive impulse (the area under the positive portion of the pressure-time pulse) were measured by subjecting a one-eighth scale, overstrong geometric model of one explosive-processing bay to internal blast loading. The use of an overstrong model for reflected pressure and impulse measurements is not new,[4] and is based on the premise that the structural response does not affect the blast reflection process as is the case for the relatively small deflections observed in the structural model tests. In addition to the impulse, we measured external shock overpressures caused by venting the explosion through the blowout panel in an area adjacent to the model blowout panel; these values were to be used to

establish personnel hazard areas in the actual processing building.

The overstrong model geometrically simulated the inside surfaces of a processing bay and was made of 3/4-in.-thick steel boiler plate. The model was drilled and tapped to accommodate reflective blast gages (see Section IV) embedded in the walls and roof so that their pressure-sensing surface was flush with the model's inside surface. The spacing of the transducer mounting holes was such that an adequate map of the peak internal reflected pressure and impulse produced by the internal blast could be obtained; for instance, the transducer mounting holes in the roof panel were centered on 8-in. squares. The external overpressure field was measured by Atlantic Research Corporation blast gages; the location and orientation of the gages referenced to the scale-model processing bay are shown in Figs. 24 and 25 (full-scale distances are found by multiplying the indicated distances by eight). The scaling laws enunciated in Appendix A apply to this investigation, of course, and external and internal pressures are invariant between the model and actual situations. Since the time scales are reduced in the model by the scaling factor, the impulses calculated from the measured pressure-time pulses must be multiplied by the scaling factor (eight) to get the corresponding full-scale values.

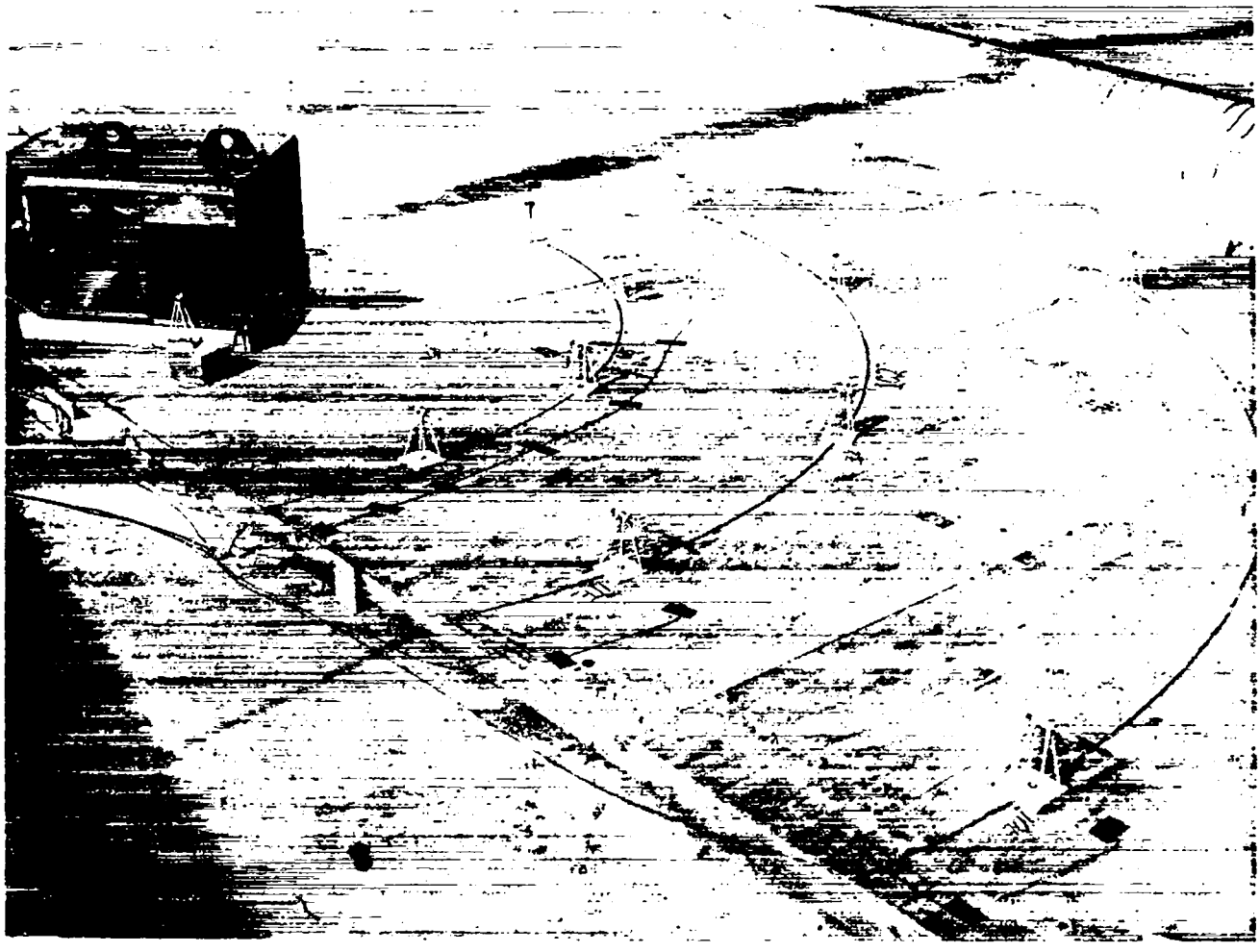

Fig. 24. The overstrong model.

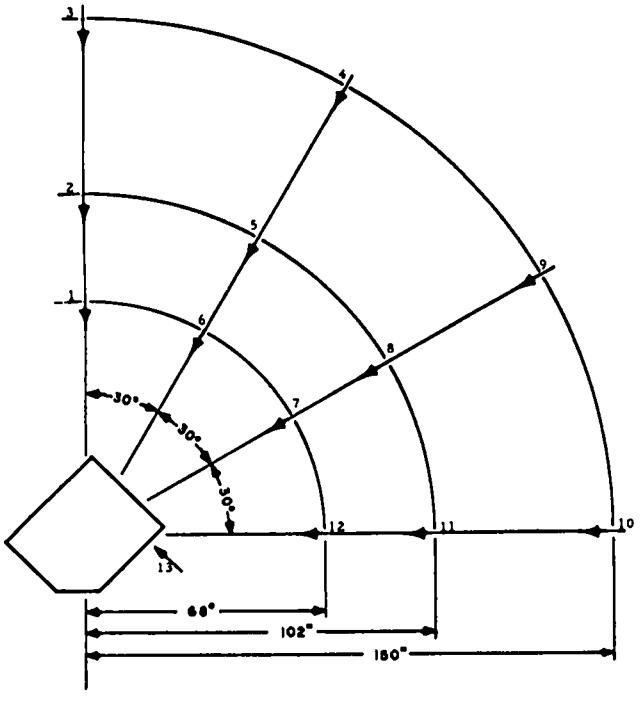

Fig. 25. Orientation of blast gages for external pressure measurements.

Table IV summarizes the tests of the overstrong model. Tests 60, 61, 62, 63, and 65 employed a blowout panel; the remaining tests did not. To prevent detonator shrapnel from flying about the inside of the model and damaging the pressure-sensing surfaces of the reflective pressure gages, the explosive charges were detonated with an MDF (mild detonating fuze) initiation system with the SE-1 detonator located outside the model. The charges were centered midway between the floor and ceiling of the overstrong model for Tests 60, 61, 66, 67, and 68, whereas in Tests 62 through 65 they were positioned a scaled 4 ft above the floor as in the structural model tests.

Figure 26 illustrates typical pressure-time traces obtained in Tests 60 through 68; the top trace is from a reflective blast gage, and the bottom from an Atlantic Research Corporation gage used to measure pressures outside the model. The areas under the reflected pressure-time traces (suitably enlarged) were determined by means of a planimeter, and provided the impulse values given in Fig. 27. The results of this testing and accompanying data analysis are as follows.

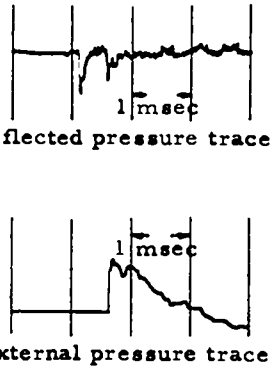

Fig. 26. Typical reflected pressure and external pressure traces.

TABLE IV

Tests of the Overstrong Model

Test	Explosive	Full-Scale Charge (lb)	Scaled Charge (g)	Charge Placement Coordinates (ft) (See Fig. 1) X	Y	Pressure Measurements
60	PBX 9404	25	22	10	12	Internal at 20 locations
61	TNT	25	22	10	12	"
62	PBX 9404	25	22	10	5	"
63	PBX 9404	25	22	10	12	"
64	PBX 9404	25	22	10	12	"
65	PBX 9404	100	88	10	12	"
66	PBX 9404	25	22	10	12	External at 13 locations
67	TNT	25	22	10	12	"
68	PBX 9404	100	88	10	12	"

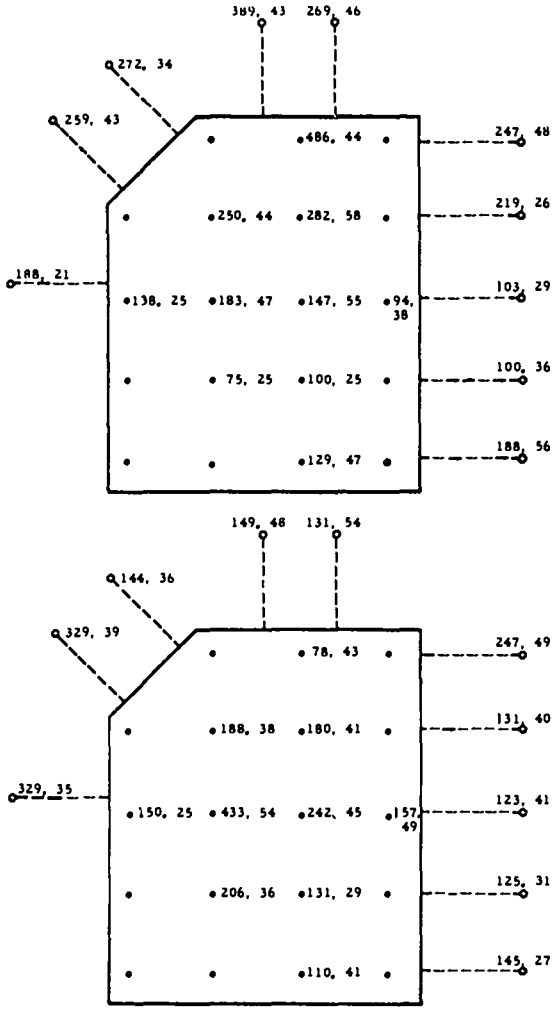

Fig. 27. Overpressure and impulse distributions in the overstrong model. Top, Test 62; bottom, Test 63. The first number at each position is peak reflected overpressure in psi, the second is reflected impulse in psi-msec.

Tests 60 and 61 compared the reflected impulse and pressure applied to the model by similarly positioned charges of the same weights of PBX 9404 and TNT. The reflected impulses measured at eight different locations on the model averaged 30% greater for PBX 9404 than for TNT. Substantially the same effect was observed in the case of reflected pressures although there was considerable scatter in the pressure data.

Tests 62 and 63 investigated the effect of charge location on the resulting peak overpressure and impulse distribution applied to the model structure. The peak overpressure and impulse distributions are shown in Fig. 27. The dashed lines lead to transducer locations on the sidewalls midway between the floor and ceiling of the model. Although there is a considerable variation in the peak reflected pressures throughout the structure, the impulse applied to the structure is seen to be fairly uniformly distributed. Impulse values were in fair agreement with those given in Fig. B3 in Appendix B and used in the calculations described there.

Test 64 again tested the hypothesis that the blowout panel had little effect on the response of the structural models. Little difference was observed between the peak reflected overpressures and impulses measured in Tests 63 and 64. Finally, on Test 65 we measured peak reflected overpressures and impulses produced in the structure by the 100-lb-equivalent charge of PBX 9404.

The external pressures caused by venting the explosion through the blowout panel area were measured at 13 locations in Tests 66 through 68. The peak overpressures measured in Tests 66 through 68 at the positions indicated in Fig. 25 are listed in Table V.

TABLE V

External Peak Overpressures (psi)

Position	Test 66	Test 67	Test 68
1	5.3	4.0	12.9
2	2.3	1.6	6.7
3	1.1	1.3	2.5
4	1.4	1.3	5.0
5	3.3	3.1	12.2
6	5.7	4.2	17.7
7	5.7	4.6	20.7
8	3.5	3.2	15.2
9	2.0	1.8	7.7
10	1.3	1.0	6.3
11	2.9	2.3	11.0
12	5.2	4.2	16.6
13	15.5	11.6	86.0

As expected, the overpressure field depends strongly on the distance from the charge. Some shielding from overpressure by the walls of the model bay is indicated by somewhat lower pressures recorded along the edges of the quadrant of Fig. 25. Overpressures recorded in Test 67 for a TNT charge were somewhat lower (10 to 20%) than those recorded in Test 66 for the same weight

of PBX 9404. We also compared the external pressures measured in Tests 66 and 67 with pressures computed from the Explosion Effects Data Sheets[7] for unconfined, spherically divergent explosions. For equivalent explosive weights of TNT at equivalent distances these computed values are:

Explosive Weight	Pressure at 46 ft (68 in.)	Pressure at 69 ft (102 in.)	Pressure 100 ft (150 in.)
25 lb TNT	3.6 psi	1.7 psi	1.1 psi
100 lb TNT	9.8 psi	3.5 psi	2.0 psi

Overpressure values measured in Tests 66 and 68 were about twice those given by the Explosion Effects Data Sheets; this we attribute to the effects of the use of a high energy explosive and to the confinement provided by the processing bay so that the explosive energy is expended directionally through the blowout-panel area.

APPENDIX A

THE SCALING LAWS

Certain nondimensional factors or constants often appear in the basic differential equations describing physical processes, after the introduction of dimensionless independent and dependent variables. All solutions of the basic equations are then similar for the same values of these constant factors (as the basic equations are identical) with the result that a great deal of generality is achieved for the same amount of computing effort. Fluid mechanics provides numerous examples of dimensionless factors, the Mach number, Reynold's number, and dynamic pressure coefficient being particularly well-known. The number and form of the dimensionless constants undoubtedly depend on the complexity of the basic equations needed to describe the process, and will, in turn, determine what forms of scaling are possible.

The scaling laws for a shocked fluid such as air are embodied in the so-called similarity principle.[6] This principle states that the pressure and other properties of the shocked fluid are unchanged if the time and length scales are changed by the same factor as the dimensions of the explosive loading source; e.g., the overpressure from a 1000-lb charge of TNT measured 100 ft from the charge is identical with that from 1 lb of TNT at 10 ft, but lasts ten times as long. The assumptions inherent in such scaling are that heat conduction and viscous effects are negligible everywhere but in the shock itself and that gravity effects are negligible everywhere. This scaling law is easily verified by examining the partial differential equations of conservation in continuous fields of flow and the Rankine-Hugoniot equations expressing conservation of mass, momentum, and mechanical energy of a fluid element passing through a shock wave. The similarity principle has been shown by experiment to be valid for detonations of explosives in air and water over a large range of explosive-charge weights and distances.[9]

The scaling laws for structural response can also be obtained by examining the basic differential equations that describe the response.[10] Here, however, we proceed in the conventional (and more general) engineering style. Although our results apply to more general rate-independent constitutive relations, we assume for simplicity that the overall mechanical behavior of the structural material is characterized by elasticity with an effective elastic modulus, E (in psi), and a perfectly plastic behavior with yield strength, σ_o (in psi), or by brittleness with a breaking strength of σ_o or by a combination of these characteristics; strain-rate (or stress-rate) effects are neglected. Typical stress-strain curves for the ductile material (reinforcing bar) and for the brittle material (concrete) are shown in Fig. 2 in the body of the report. If we also assume that the structure is one-dimensional, as is the case for a simple beam, the dynamic response of the structure can be expressed in the form

$$u(x, t) = f(\ell, x, E, \sigma_o, \rho, p, t_o, t, \psi_s, \psi_p) \qquad (A1)$$

where u(x, t) is the structural deflection measured at point x on the structure at time t. (For more general structures u, x, and f are vectors.) The deflection, u, is caused by a pressure, p (in psi), applied to the structure over a time interval, t_o; the pressure distribution over the structure is specified by the dimensionless factor ψ_p. Note that p = p(x, t), and, in essence, ψ_p indicates the dependence of p on x. The quantity ρ is the mass density (in lb-sec^2/in.^{4}), ℓ is a typical structural

dimension (such as beam length), and φ_s is a dimensionless shape factor for the structure which relates all other structural dimensions to ℓ (e.g., beam thickness-to-span ratio). From dimensional analysis* we can write

$$\frac{u(x,t)}{\ell} = F\left(\frac{\sigma_o}{E}, \frac{p}{E}, \frac{t}{t_o}, \frac{pt_o^2}{\rho\ell^2}, \frac{x}{\ell}, \varphi_s, \varphi_p\right). \qquad (A2)$$

To accomplish scaling with complete similarity, the dimensionless products in the right-hand side of Eq. (A2) must have the same values for the model as for the actual or prototype structure. We observe first that we must hold φ_s, the shape factor, the same in the model and prototype which is termed geometric scaling. If the model and prototype are constructed of the same materials, the quantity σ_o/E will be identical in both (as will be ρ, the mass density). Suppose that the explosive-charge dimensions are reduced as the geometric scaling factor between model and prototype and the explosive charge is located at corresponding positions in both. Then, by the similarity principle for explosives, p/E, φ_p, and $pt_o^2/\rho\ell^2$ will be identical in the model and prototype because p is identical at the scaled position and t_o is scaled as the length scale (provided, of course, that the same fluid and explosive are used for the shock process). Thus, at corresponding values of t/t_o and x/ℓ, F becomes a function of the same constants and u/ℓ is identical in the model and prototype. Since strain is dimensionless, the strain (and consequently the stress) is identical in model and prototype at scaled times and positions as is structural damage, provided that the damage is not rate-dependent. An experimental verification of this scaling principle for large deflection elastic and plastic response of cantilever beams to blast loading is given by Baker.[10]

The initial stress field produced by the weight of the structure itself and the effects of strain rate are not included in the scaling. The effect of the initial stress field is slight because the dynamic stresses developed in the structure are usually much greater than the initial stresses, while strain-rate effects are not pronounced for conventional (nonviscous) structural materials and for reasonable scaling factors of not less than 1/20.*

We emphasize again that in the absence of rate effects and heat conduction, the correct scaling for blast and structural simulation is purely geometric; the size and placement of the explosive is reduced by the model scaling factor.

*Buckingham's theorem states that a dimensionally homogeneous equation can be reduced to a relationship among an independent set of dimensionless products. If n variables are functionally related by an unknown dimensionally homogeneous equation, then Buckingham's theorem states that the relationship can be expressed by n-r dimensionless products.[11] In most cases r is equal to the number of fundamental dimensions in the problem; in our case there are three dimensions - length, time, and force. Since Eq. (A1) is a dimensionally homogeneous relation among 11 variables, the form of the relationship can be reduced to an expression involving 8 dimensionless products.

APPENDIX B

CALCULATION OF ELASTIC-PLASTIC PANEL RESPONSE TO BLAST LOADING

A structural model of an elastic, perfectly plastic reinforced concrete panel is described, and a numerical solution for its response to blast loading is given. The calculated blast-loading response of a rectangular panel built-in on three sides and free on the fourth is compared with the structural response measured in the scale models. The techniques used to predict the structural response are not new and are largely described in Reference 13 although we have included in our analysis the elastic portion of the structural response.

Since the response of a single-degree-of-freedom, linear spring-mass system is particularly well known, it is customary in shock and vibration analysis to replace the complex multi-degree-of-freedom structure with a single-degree-of-freedom, spring-mass system, such as the one shown

*Conventional spallation criteria include a rate effect. A common relation between spall stress, σ_s, and stress rate, $\dot{\sigma}$, is

$$\sigma_s = A\dot{\sigma}^{\frac{1}{2}} + \sigma_o ,$$

where A and σ_o are experimentally determined constants for each material and other criteria are formulated in terms of the stress gradient. For a discussion of these and other criteria see Thurston and Mudd.[12]

in Fig. B1a. The sliding connection at the end of the spring limits the spring force to an amount R and represents the ultimate resistance of an elastic, perfectly plastic structure. Under static loading (P(t) varies slowly with time), the load deflection is shown in Fig. B1b and is seen to be identical with that of an elastic, perfectly plastic rod in a state of one-dimensional stress.

The parameters of a single-degree-of-freedom system such as the mass M and spring constant k were chosen to best simulate the response of the more complex structure. The determination of M is relatively straightforward; we then chose the value of the spring constant k so that the fundamental resonance of the reinforced concrete panel (which can be estimated by calculation or measured by experiment) was duplicated in the single-degree-of-freedom system. The value of viscous damping was included primarily for calculation.

The value of R, the ultimate resistance of the panel, was determined from yield-line theory for rectangular, rigid, perfectly plastic plates.

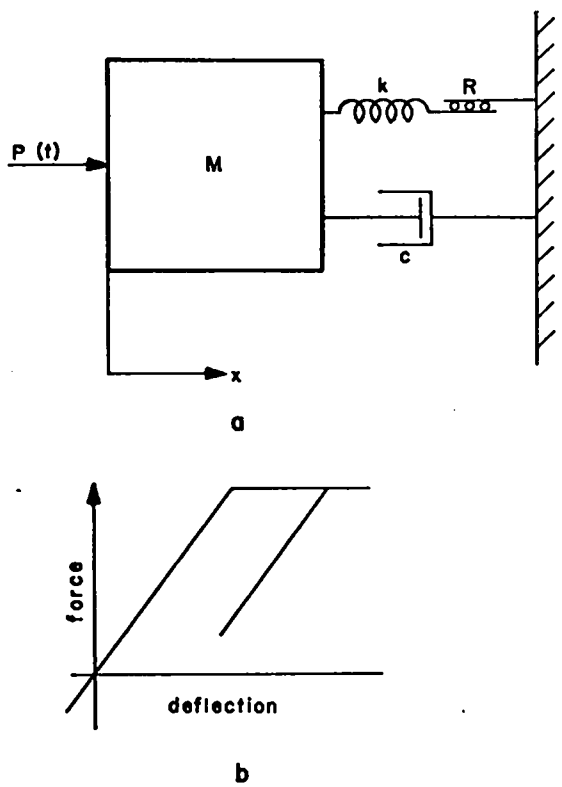

Fig. B1. Spring-mass model and load-deflection behavior under static loading.

According to the yield-line theory, a rectangular plate at collapse deforms at a constant load, with plastic deformation (characterized, in general, by points of maximum stress) confined to hinge lines of the plate, while the rest of the plate is rigid and rotates about these hinge lines. The hinge lines are called "yield lines" in the literature and are so arranged on the plate as to allow the deforming plate to operate as a mechanism. Methods for determining yield-line patterns for rectangular plates with various support conditions are discussed in References 13 and 14, and we give here only the yield-line pattern for an approximately square plate built-in on three sides and free on the fourth as shown in Fig. B2. The yield-line pattern agrees very well with the pattern developed on the roof panel during the scale-model structural tests as shown in Figs. 13 and 14.

The loading function, P(t), acting on the panel was determined from the explosively generated pressures and durations of positive pressure acting on it. Values of overpressure and duration of positive pressure were taken from the Explosive Effects Data Sheets[7] with a 60% increase in overpressure being allowed for the high explosive PBX 9404 in relation to TNT overpressures. The applied pressures were determined at the point on the panel nearest the explosive, and normal reflection of the pressure pulse was assumed. Preliminary calculations showed that the durations of positive reflected pressure were so short in

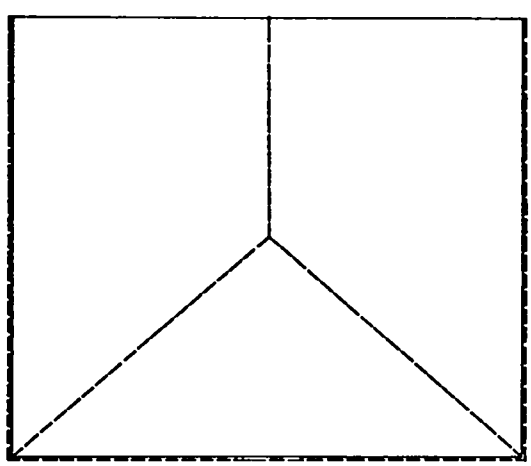

Fig. B2. Yield-line pattern for a plate built-in on three sides and free on the fourth.

relation to the natural period of the panel that impulse alone predicted the structural response with little loss in accuracy, and impulse was used in most response calculations. The reflected impulse was again determined by using the shortest straight-line distance of the panel from the explosive charge, and this value was assumed to act uniformly over the panel. Since we were neglecting multiple reflections of the blast pulse, we felt that this was an adequate approximation to the actual situation. Reference 6 provided a source of reflected impulse data for spherical Pentolite explosive charges, and a one-third increase in impulse was allowed for the high energy explosive PBX 9404. Since these data (adjusted for PBX 9404) were used often in calculations, we show the impulse data as a function of the scaled distance $R/W^{\frac{1}{3}}$ in Fig. B3; R is the distance between the panel and the explosive in feet, and W is the weight of PBX 9404 in pounds.

The differential equations describing the motion of the spring-mass system shown in Fig. B1a were integrated by Runge-Kutta numerical integration, with the structural parameters of the roof panel of the model processing bay as an example. The natural frequency of the panel was calculated to be approximately 250 cps. The response records at low charge levels in the scale-model tests showed a fundamental resonance at approximately 170 cps for the roof panel; this value was used to determine the value of k in the spring-mass system. The ultimate resistance of the model roof panel per unit area was computed from yield-line analysis and found to be 33 psi. Viscous damping of 20% of critical was assumed for the single-degree-of-freedom system. For initial conditions we took specified velocity computed from the appropriate impulse value and zero initial displacement.

Figure B4 shows the typical displacement, velocity, and spring-force response curves obtained in this fashion when an 88-gram test charge of PBX 9404 (equivalent to 100 lb in the actual structure) was detonated 12 in. from the center of the model roof panel. Finally, the solid curve of Fig. 19 summarizes the computations of maximum roof-panel displacement as a function of the eqivalent charge weight of PBX 9404 detonated in the full-scale structure. The computed values agree well with the deflection values obtained during the scale-model tests.

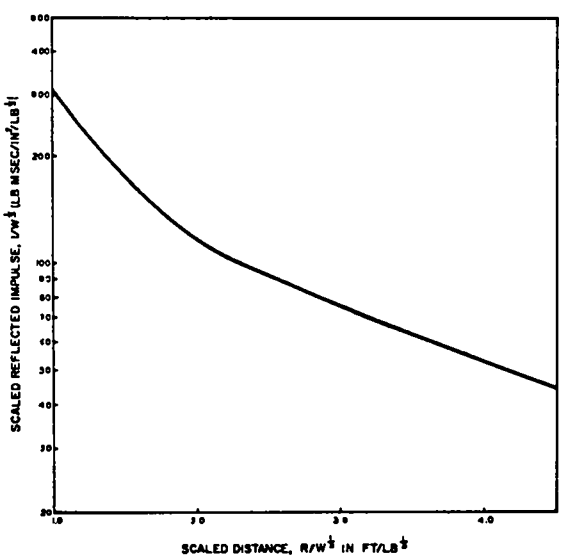

Fig. B3. Reflected scaled impulse vs scaled distance data taken from Reference 6 and adjusted for PBX 9404.

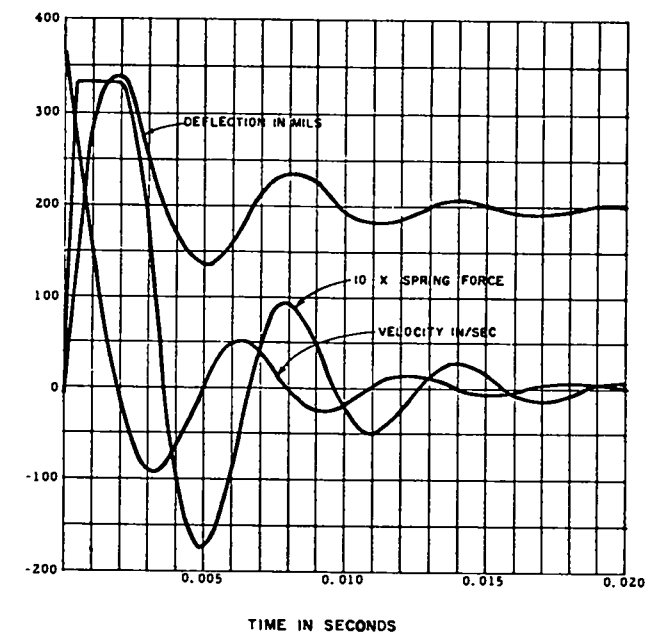

Fig. B4. Typical computed displacement, velocity, and spring-force response curves.

ACKNOWLEDGMENTS

The study reported here originated in 1960-61, and since then many people at GMX-3 have contributed their efforts to it. In particular, the author thanks G. S. Dow, Jr., N. K. Kernodle, R. W. Mathews, E. A. Pacheco, and B. W. Deitrick for their cooperation in ensuring that this study reached a successful conclusion.

REFERENCES

1. S. Glasstone, The Effects of Nuclear Weapons, (USAEC Washington, D.C., 1962), Chapter IV.

2. Technical Information Division, USAEC, "The Effects of Atomic Weapons on Structures and Military Equipment," Foreign Weapon Effects Reports, July, 1954. USAEC, Wash. Report FWE-8 (Secret).

3. S. Wachtell and R. Rindner, "A Manual for Design of Protective Structures Used in Explosive Processing and Storage Facilities," Summary presented at the 10th Annual Safety Seminar, Louisville, Kentucky, August 13-15, 1968.

4. W. G. High, "The Design and Scale Model Testing of a Cubicle to House Oxidation or High Pressure Equipment," Chem. Ind. (London), 898, June 30, 1967.

5. C. S. White and D. R. Richmond, "Blast Biology," Lovelace Foundation Report TID-5764, September 18, 1959.

6. O. Johnson, W. Olson, and J. Patterson, "A Simple Mechanical Method for Measuring the Reflected Impulse of Air Blast Waves," Proc. Third U.S. Natl. Cong. Appl. Mech., American Society of Mechanical Engineers, New York, 1958.

7. E. A. Christian and E. M. Fisher, Explosion Effects Data Sheets, Naval Ordnance Laboratory Report NAVORD 2986, June 1955.

8. R. H. Cole, Underwater Explosions, (Princeton University Press, New Jersey, 1948).

9. R. S. Stover and W. Bleakney, "The Attenuation of Spherical Shock Waves in Air," J. Appl. Phys. 19, 670 (1948).

10. W. E. Baker, "Modeling of Large Transient Elastic and Plastic Deformations of Structures Subjected to Blast Loading," J. Appl. Mech. 27, 521 (1960).

11. H. L. Langhaar, Dimensional Analysis and Theory of Models, (John Wiley and Sons, Inc., New York 1951).

12. R. S. Thurston and W. L. Mudd, "Spallation Criteria for Numerical Computations," Los Alamos Scientific Laboratory Report LA-4013, November 1968.

13. Armour Research Foundation, "Investigation of Sympathetic Detonation and Evaluation of Structures for Ammunition Manufacture," Final Report, Part II, November 8, 1955.

14. E. Hognestad, "Yield-Line-Theory of the Ultimate Flexural Strength of Reinforced Concrete Slabs," J. Am. Concrete Inst. 24, 651 (1953).